Progress In Electromagnetics Research, Vol. 177, 1–20, 2023

Topological Edge Modes in One-Dimensional Photonic Artificial Structures

Jiajun Zheng, Zhiwei Guo, Yong Sun*, Haitao Jiang*, Yunhui Li, and Hong Chen*

(*Invited Paper*)

Abstract—In recent years, topological states in photonic artificial structures have attracted great attention due to their robustness against certain disorders and perturbations. To readily understand the underlying principles, topological edge modes in one-dimensional (1D) system have been widely investigated, which bring about the discovery of novel optical phenomena and devices. In this article, we review our recent advances in topological edge modes. We introduce the connection between topological orders and effective electromagnetic parameters of photonic artificial structures in band gaps, discuss experimental demonstration of robust topological modes and their potential applications in wireless power transfer, sensing and field of optics, and give a brief introduction of future opportunities in 1D topological photonics.

1. INTRODUCTION

In recent years, a new state of matter called topological insulator (TI) has been a hot topic in the field of condensed matter physics [1, 2]. Despite insulating in the bulk, electrons can move along the surface of a TI without backscattering even in the presence of large impurities, which is called topological edge mode (TEM). It has been verified that TEMs are protected by the bulk band topology of TI.

The concept of TI was soon introduced into various photonic structures like photonic crystals (PCs) and metamaterials [3]. The idea of photonic TI (PTI) was first proposed by Haldane in 2005 [4]. By introducing magnetic field into a gyromagnetic photonic crystal, Wang et al. observed the photonic analogue of quantum Hall effect in photonic structure [5]. This is the first experimental demonstration of the topologically protected one-way waveguide with little backscattering, which represents a milestone in the development of topological photonics. In addition, PTIs without breaking time-reversal symmetry were proposed later, including PTIs with synthetic magnetic fields [6], PTIs with carefully designed magneto-electric coupling [7], and PTIs with pseudo-time-reversal symmetry [8]. These fundamental researches in PTI spark many novel designs, such as TI laser [9, 10], photonic graphene [11], and Dirac-vortex topological photonic crystal fiber [12].

PC is the optical analogue of the crystal in which the electromagnetic parameters change periodically [13]. Similar to the band of the crystal, the band structure of PC originates from periodic scattering of light, and electromagnetic modes are evanescent inside the gap. PCs are employed in suppression of spontaneous emission and light manipulation [14, 15]. As a typical artificial photonic microstructure, PC has attracted great interest because the electromagnetic response of a PC can be manipulated by tailoring geometry of the unit cell. The simplest PC consists of alternating layers of

Received 12 October 2022, Accepted 18 January 2023, Scheduled 13 February 2023
* Corresponding authors: Yong Sun (yongsun@tongji.edu.cn), Haitao Jiang (Jiang-haitao@tongji.edu.cn), Hong Chen (hongchen@tongji.edu.cn).
The authors are with MOE Key Laboratory of Advanced Micro-Structured Materials, School of Physics Science and Engineering, Tongji University, Shanghai 200092, China.

material with different dielectric constants, which is often called multilayer film. Besides, a quasi 1D structure composed of a backbone waveguide and side-coupled resonators is reported to have band structures similar to a PC [16]. PCs have broad applications [13] like PC waveguide, PC laser, PC cavity, and PC fiber.

Metamaterial is another kind of artificial photonic microstructure in subwavelength scale [17]. Due to the subwavelength nature of its unit cells, the electromagnetic properties of a metamaterial can be characterized by local permittivity ε and permeability μ according to effective medium theory. Metamaterials can achieve negative ε or μ that can be rarely found in materials in nature, which can be classified into single negative materials (SNGs) and double negative materials. Pendry proposed a negative-μ metamaterial consisting of spilt ring resonators (SRRs), and such a design is experimentally realized later in 2000 [18]. In 2001, another metamaterial in microwave regime based on theory of transmission lines (TLs) was proposed, which are expected to have broader band and lower loss than SRRs [19]. Metamaterials have aroused great attention because the arbitrarily designable ε and μ enable one to manipulate electromagnetic wave at will [20–22]. Today, metamaterials have a variety of applications with great potential such as coding metasurfaces [23], broadband antenna [24], polarization, and wave front manipulation [25, 26].

1D Su-Schrieffer-Heeger (SSH) chain is the simplest model to exploit topological modes [27]. Topological transition can be observed with the change of coupling between sites of the unit cell. Topological mode with zero energy protected by the chiral symmetry condition can emerge at the end of an open chain with nontrivial topology or the interface between two SSH chains with different band topology. The electromagnetic properties of photonic artificial microstructure can be flexibly controlled through the engineering of geometry, so we can expect that photonic artificial microstructure provides a versatile platform for investigating topological modes of PTI [28–34].

In this article, we review the recent advances on TEM of 1D photonic systems in our group. We first examine the band topology and TEMs from the point of view of effective medium theory in multi-scattering photonic artificial structures including PCs, TL metamaterials, and locally resonant metamaterials. We then discuss the experimental observation of robust TEMs and direct measurement of topological invariant in dimerized resonator (SRRs and resonant coils) chain based on tight-binding model. Potential applications of TEMs in wireless power transfer, sensing, and field of optics are also highlighted. Finally, we give a brief introduction of future opportunities in 1D topological photonics.

2. THE EFFECTIVE ELECTROMAGNETIC PARAMETERS FOR TOPOLOGICALLY DISTINGUISHABLE PHOTONIC BAND GAP FROM MULTI-SCATTERING

2.1. Photonic Simulation of Dirac Equation in 1D Topological Metamaterial

The Dirac equation provides a description of relativistic quantum mechanics for elementary spin-1/2 particle, which has extensive applications in condensed matter physics. It is found that effective Hamiltonians for the quantum spin Hall effect have an identical mathematical structure of the Dirac equation, implying that each TI is governed by one Dirac equation [35]. In electromagnetism, light wave propagation is governed by Maxwell's equations. When it comes to characterization of topological properties for 1D photonic system, it is of great significance to build a bridge between the Dirac equation and Maxwell's equations.

Tan et al. first gave a concrete example to support the idea that Maxwell's equations of electromagnetism can be explicitly mapped to the Dirac equation in one dimension [29].

A 1D plane electromagnetic wave can be described by Maxwell's equations

$$-\partial_x E_z = i\omega\mu(x) H_y \tag{1a}$$

$$\partial_x H_y = -i\omega\varepsilon(x) E_z \tag{1b}$$

Here, E_z and H_y are the electric and magnetic fields. By introducing the spinor $\varphi = \begin{pmatrix} \sqrt{\varepsilon}_0 E_z \\ \sqrt{\mu}_0 H_y \end{pmatrix}$.

Equations (1a) and (1b) can be written in the form of the Dirac equation

$$[-i\sigma_x\partial_x + m(x)\sigma_z + V(x)]\varphi = E\varphi. \tag{2}$$

Here, $m(x) = \frac{\omega}{2c}[\varepsilon_r(x) - \mu_r(x)]$, $V(x) = \frac{\omega}{2c}[\varepsilon_r(x) + \mu_r(x) - \langle\varepsilon_r(x) + \mu_r(x)\rangle]$ are the effective mass and potential, respectively; $E = -\frac{\omega}{2c}\langle\varepsilon_r(x) + \mu_r(x)\rangle$ is the energy eigenvalue; c is the speed of light in vacuum; $\sigma_{x,y,z}$ are the three Pauli matrices; and the Planck constant $\hbar$ and c are taken as units. In this way, the rigorous relation between the effective mass m of the Dirac equation and the effective permittivity ε and permeability μ is established.

Such relation is demonstrated in TL metamaterials, which is shown in Figs. 1(a) and 1(b). With the width w of TLs changing, the effective mass transits from positive value to negative value, and the closing and reopening of the gap can be observed. Such band inversion process is also known as topological transition in SSH model. Furthermore, as shown in Figs. 1(c) and 1(e), a heterostructure composed of 2 TLs with different signs of m is fabricated, and an interface mode can be observed, which is a realization of Jackiw-Rebbi solution as well as a TEM.

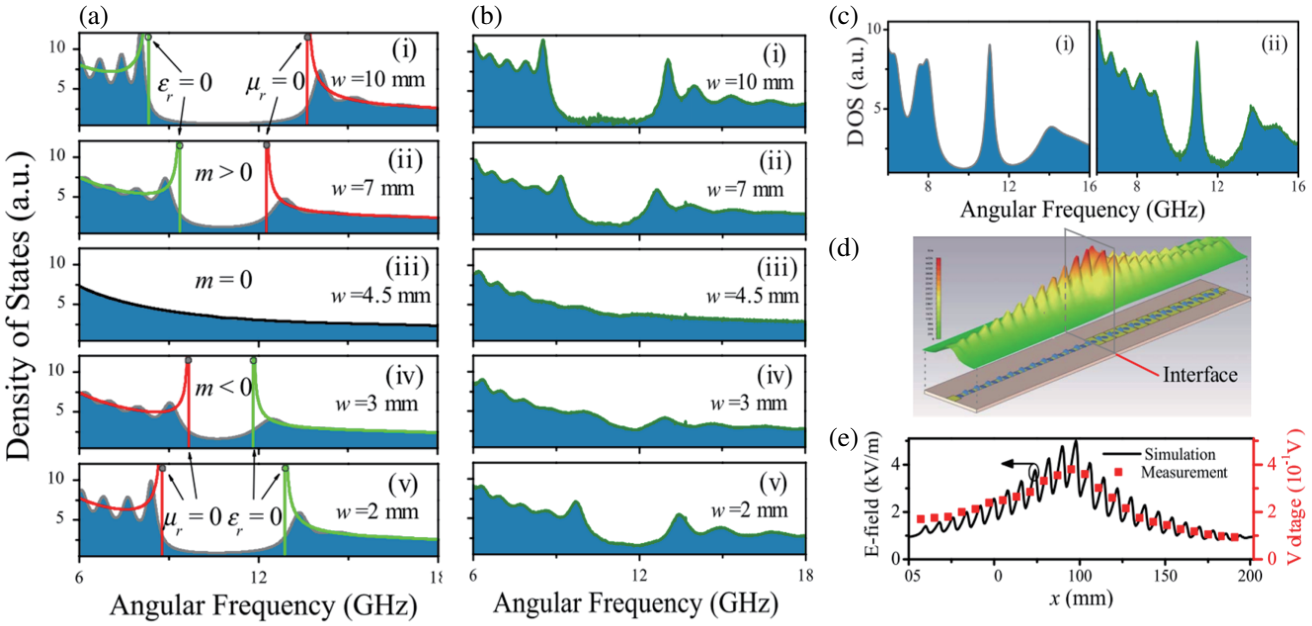

Figure 1. Photonic simulation of band inversion in the Dirac equation and TEM in the heterostructure. (a) Calculated density of states (DOSs) for microwave TL samples with losses. The solid (red) lines are the DOS spectra for ideal structures without losses. (b) Measured DOS for microwave TL samples. (c) Calculated (i) and measured (ii) DOS spectra of heterostructure composed of components with opposite masses, exhibiting a TEM within the gap. (d)–(e) Simulated (d) and measured (e) field distribution of the TEM. The two components are designed with $w_1 = 2.5\,\text{mm}$ and $w_2 = 8.5\,\text{mm}$, respectively. Reproduced with permission from [29]. Copyright 2014 Springer Nature. CC BY-NC-ND 3.0.

Apart from aforementioned work based on 1D metamaterials, the connection between Dirac equation and topology has been extensively investigated in 2D photonic systems like metacrystals [7], photonic graphene [8], and waveguide lattice [11]. These pioneering works provide paradigms for the research on 2D topological photonics.

2.2. Effective Electromagnetic Parameters for Topologically Distinguishable Band Gaps of 1D Photonic Crystals

The connection between effective electromagnetic properties of SNGs and band topology has been established. Notably, it has been shown that modes are evanescent in the band gap of both PCs and SNGs, implying that PC and SNG may have similar band topology.

To investigate topological PCs from the perspective of effective electromagnetic parameters, the feasibility of applying effective medium theory to gaps of PCs must be verified first. In 2006, Guan

et al. [36] found that topological mode with zero volume exists at the interface between two different PCs under condition $\bar{\varepsilon} = \bar{\mu} = 0$ ($\bar{\varepsilon}$ and $\bar{\mu}$ represent average electromagnetic parameters of the whole heterostructure), which explicitly implies that MNG gap of the PC $(AB)_N$ on the left and ENG gap of the PC $(A'B')_N$ on the right correspond to different topology orders [36]. In Fig. 2, $\bar{\varepsilon_1}$, $\bar{\mu_1}$ represent electromagnetic properties of PC $(AB)_N$, and $\bar{\varepsilon_2}$, $\bar{\mu_2}$ represent electromagnetic properties of PC $(A'B')_N$. Topological tunneling mode can be seen in Fig. 2(c). Besides, with the length of dielectric layer d_A, d_B changing, inversion of band edge is clearly illustrated in Figs. 2(a) and 2(b). Before band inversion, the edge of $\bar{\mu_1} = 0$ is located at high frequency while the edge of $\bar{\varepsilon_1} = 0$ is located at low frequency. The two edges are exchanged with each other after the inversion process.

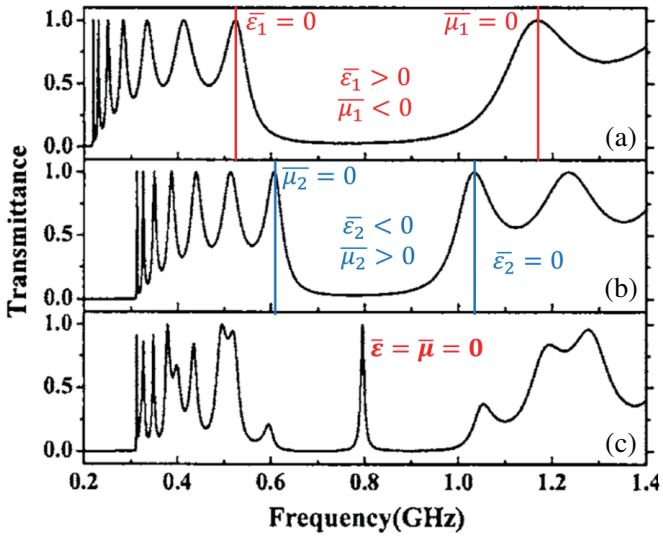

Figure 2. Transmittances through the single photonic crystals and the heterostructure. (a), (b), and (c) refer to $(AB)_8$, $(A'B')_8$, and $(AB)_8\,(A'B')_8$, respectively. Reproduced with permission from [36]. Copyright 2006 AIP Publishing.

Subsequently, Guo et al. proposed that the photonic band gap (PBG) structure can mimic SNG material, that is to say, a PBG structure may be treated as a homogenous material with negative ε_{eff} or μ_{eff} [37]. Further study indicates that effective parameters of PCs with symmetric unit cells are independent of the number of periods.

Based on these works, Shi et al. developed a simple method to calculate ε_{eff}, μ_{eff} of PCs in gaps with symmetric unit cells [38]. A close relation between sign change of ε_{eff}, μ_{eff} and reflection phase can be observed in Fig. 3(a). Topological properties of the gaps can thus be determined by the method of mapping Maxwell's equations to Dirac equation mentioned above.

Similarly, a heterostructure composed of 2 PCs with different topologies is fabricated, and a TEM robust against disorders emerges at the interface (Figs. 3(b), 3(c)). The mode is protected by a zero average effective mass condition $\bar{m} = 0$ corresponding to chiral symmetry condition in SSH model, which is illustrated in Fig. 3(c). In other words, the condition $\bar{m} = 0$ is a criterion whether the disorder implemented may corrupt the robustness of 1D TEM. In 2D topological photonic systems, it is challenging to analyze the effect of disorders on TEMs quantitatively. As shown in Fig. 3(d), transmittance of the interface state is significantly reduced when the $\bar{m} = 0$ condition is broken.

Later, Guo et al. extend the concept of optical topological manipulation to the short-wavelength region. Such TEM protected by $\bar{m} = 0$ condition is experimentally demonstrated in the X-ray regime [39]. The fabricated structure is shown in Fig. 3(e) where C and W represent carbon and tungsten layers, respectively, along with PC_A and PC_B denoted by $(\mathrm{CWC})_{10}$ and $(\mathrm{WCW})_{10}$. It can be seen from Fig. 3(f) that a reflectance dip in the common gap of PC_A and PC_B indicates the existence of TEM. The observation of TEM in X-ray regime may pave the way for high-precision optics and robust devices against structural perturbations.

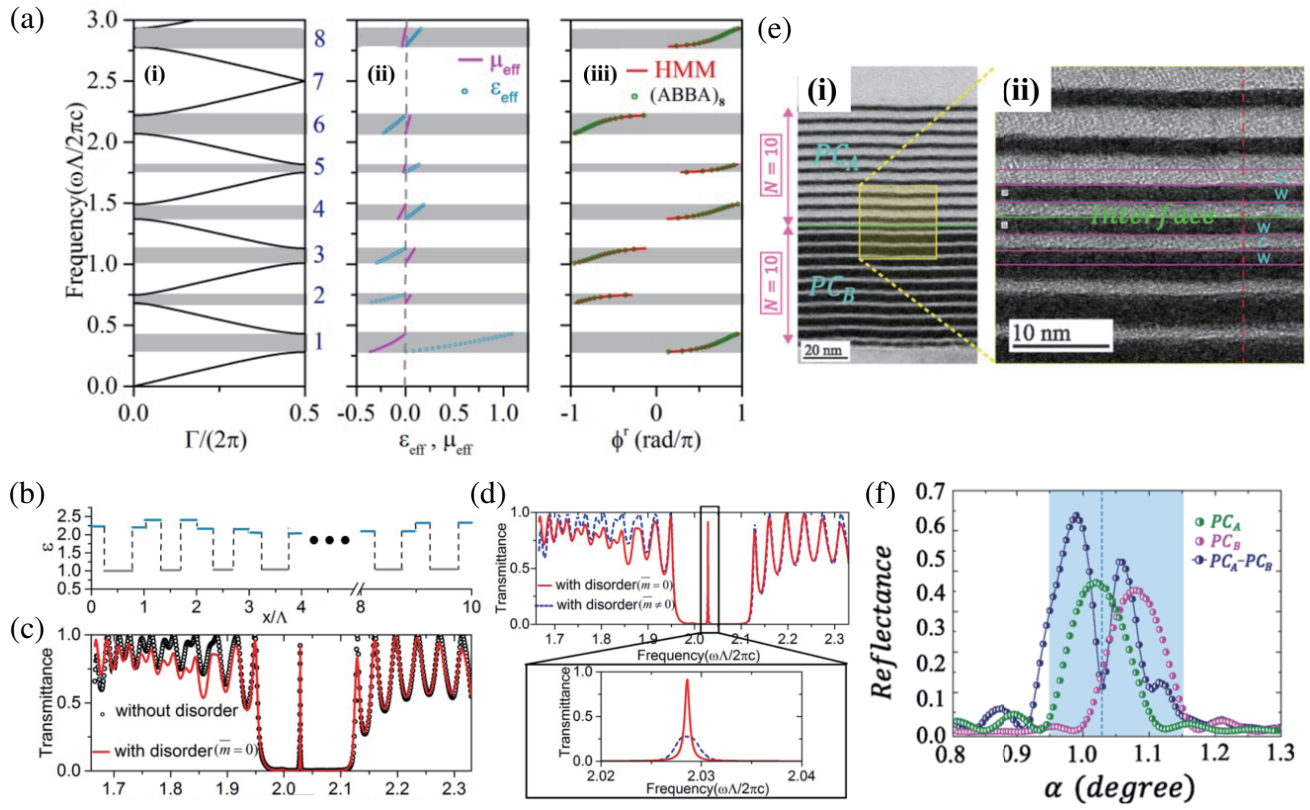

Figure 3. The retrieved ε_{eff}, μ_{eff}, and reflection phase of the PC, and TEM in the PC heterostructure. (a) The retrieved ε_{eff}, μ_{eff}, and reflection phase of the PC. (i) The band structure of the infinite-periodic PC $(ABBA)_N$. Γ denotes the Bloch phase. (ii) ε_{eff} and μ_{eff} of the structure for frequencies within the gaps. (iii) Reflection phase spectra of $(ABBA)_8$ and the homogenized material with same thicknesses, respectively. (b) The randomness configuration introduced in the SNG PTI. The $\bar{m} = 0$ condition is satisfied for the heterostructure. (c) Transmittance spectra of the heterostructures satisfying $\bar{m} = 0$. (d) Transmittance spectra of the heterostructures with disorders. A magnification is given for a better view. (e) Experimental design of the cross-section of the fabricated PC_A–PC_B structure. An enlarged image of the interface area is shown in (ii), in which the interface of PC_A and PC_B is marked by the green line. (f) The measured reflectance of the individual structures, PC_A and PC_B, and the composite structure PC_A–PC_B with respect to different incident angle at the frequency of TEM. (a)–(d) Reproduced with permission from [38]. Copyright 2016 The Optical Society. (e)–(f) Reproduced with permission from [39]. Copyright 2019 WILEY-VCH Verlag GmbH & Co. KGaA, Weinheim.

Alternatively, topological property of PC can be determined from the point of view of Zak phase. In 2014, Xiao et al. introduced the theory of Zak phase into photonic bands, and band inversion was observed along with the change of Zak phase, which embodies topological transition [31, 40]. In addition, the surface bulk correspondence is established, which builds a connection between Zak phase of a bulk band and reflection phases of two gaps sandwiching this band. These results are in accordance with those obtained in [38].

2.3. More Flexible Control of Band Topology in 1D Dimerized Locally Resonant Metamaterials

The manipulation of topology of PBGs plays an important role in designing 1D TEMs. A typical method is to alter the filling ratio of the components of a PC [31]. Nevertheless, it remains a problem that topological property of the lowest gap which is of great significance in subwavelength wave manipulation

is immutable by this method.

Different from the PBGs in PCs originating from Bragg scattering, there is another kind of hybrid PBGs in locally resonant metamaterials resulting from interference between continuum of guided/plane waves and local resonators [41]. Such metamaterials allow us to tailor unit cells locally to control the wave propagation in subwavelength scales.

Topological properties of a similar multi-scattering structure (without dimerization) have been exploited in acoustics in 2015 [42]. Inspired by these works, a dimerized 1D locally resonant metamaterial is proposed to adjust topology of the first gap [43].

In 2018, Zhu et al. demonstrated band inversion through tuning dimerization parameter Δ of a locally resonant metamaterial composed of a backbone waveguide and side-coupled branches, which is shown in Figs. 4(a)–4(d) [43]. TEM at the interface between two components with distinct band topology was also observed. It is notable that locally resonant metamaterials can be characterized by effective electromagnetic parameters, and the sign change of ε_{eff} (or μ_{eff}) of metamaterials in the gap is in accordance with topological transition. Further, it is shown in Figs. 4(e)–4(g) that there are some singular points associated with zero reflection in the bulk band across which the Bloch states contribute π to the Zak phase, whereas in the rest of the band the contribution is nearly zero. Due to the local resonance in such quasi 1D system, the number of singular points in the first band can be controlled by adjusting the dimerization parameter. The manipulation of the topological order of the first band is thus realized, which cannot be achieved in common 1D systems.

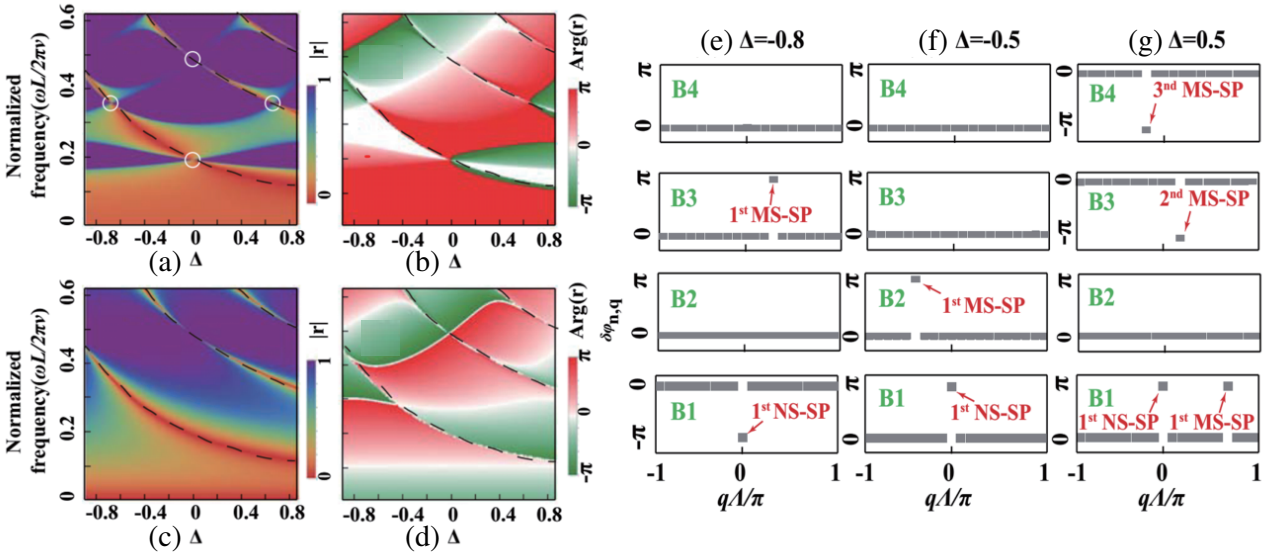

Figure 4. Band inversion and Zak phase in dimerized 1D locally resonant metamaterials. (a)–(d) Reflection coefficient for the semi-infinite systems ((a) and (b)) and single unit cell ((c) and (d)). Four topological phase-transition points are indicated by the white circles. The states with zero reflection are marked by a group of black dashed curves. (e)–(g) The contribution of singular points (SPs) in the first Brillouin zone to the Zak phases. Two types of SPs are indicated by non-scattering-induced (NS-SP) and multiple-scattering induced (MS-SP), respectively. The 1st (2nd) means the principal value (the second branch value) of the multivalued equations. Reproduced with permission from [43]. Copyright 2018 American Physical Society.

Apart from photonic structures based on multi-scattering where far-field coupling is involved, topological transition can also appear in system governed by near-field coupling such as SSH chain. It is a fascinating question how the interaction of two different couplings determines the band topology of system. Very recently, hybrid couplings containing both near-field and far-field interactions are introduced into such a dimerized structure, which is illustrated in Fig. 5(g) [44]. Band inversion is achieved by tailoring the near-field coupling in addition to dimerized parameter mentioned above, which

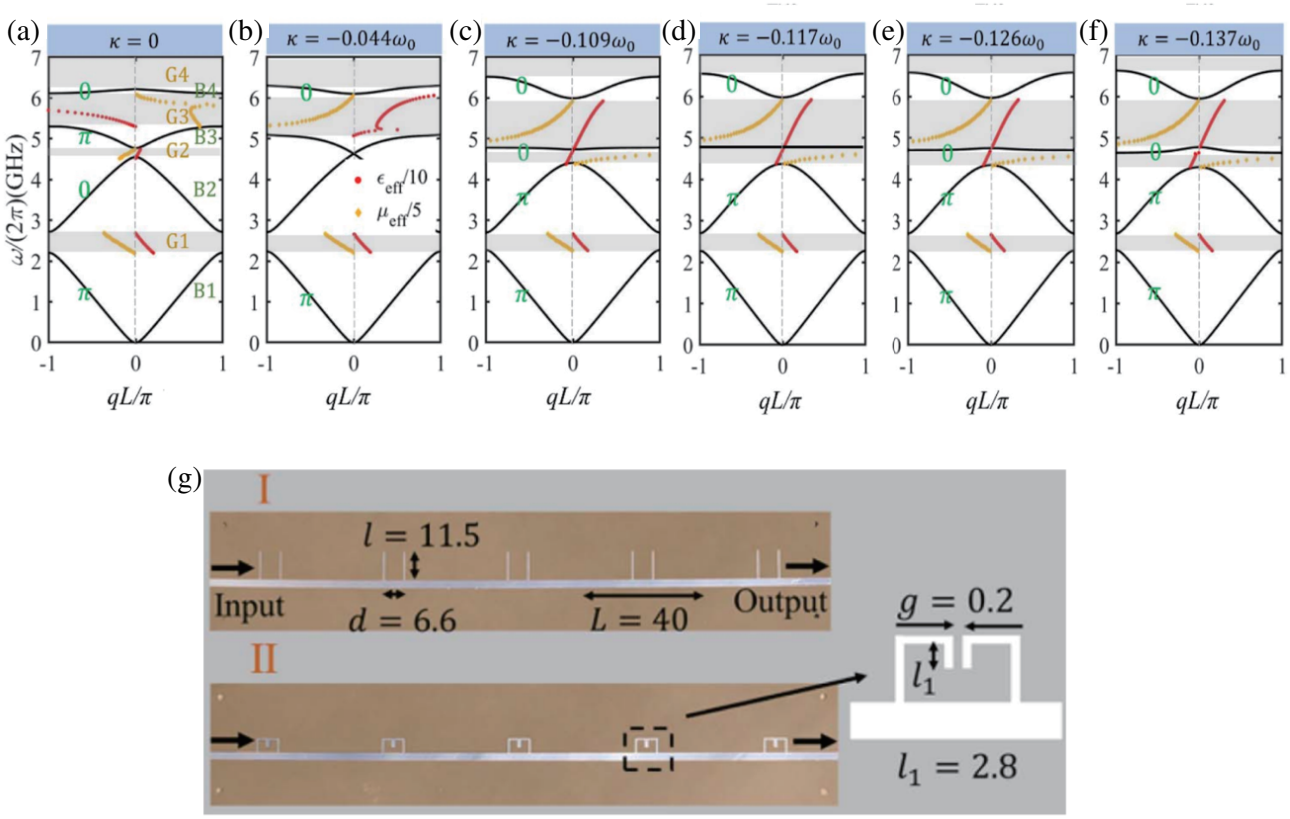

Figure 5. Topological phase transition in chain with hybrid coupling. (a)–(f) Band structures of infinite 1D dimerized chain for a fixed dimerized parameter. The Zak phases for each band are marked. (g) Samples of 1D chain with far-field coupling and chain with hybrid coupling, respectively. Reproduced with permission from [44]. Copyright 2022 Chinese Laser Press.

is shown in Figs. 5(a)–5(f). Moreover, the change in near-field coupling modulates the effective mass of photon for the upper band from positive to negative, leading to an indirect bandgap, which cannot be achieved in conventional dimerized chains with either far-field or near-field coupling only.

In addition to periodic structures mentioned above, quasiperiodic and non-periodic structures also play important roles in topological photonics [45, 46]. Particularly, it is found that non-periodic structures with long-range order can be seen as originating from periodic structures of a higher dimension, which makes it possible to explore topological properties of 2D system in 1D structure [47].

The schematic of a multi-scattering quasiperiodic structure based on Aubry-Andre-Harper (AAH) model [30] is presented in Fig. 6(a). The distance d_n between the nth and $(n+1)$th side-branch tubes is modulated as

$$d_n = d\left\{1 + \delta\cos\left[2\pi b\left(n-1\right) + \phi\right]\right\} \tag{3}$$

Here d is the unmodulated distance, δ the strength of modulation, $b = P/Q$ a rational number with P and Q being two integers with no common factors, and ϕ an arbitrary phase. It is shown in Fig. 6(b) that two TEMs localized on either end of the system exist in the gap of the band structure. The left edge mode shown in Fig. 6(b) in the second band gap can be probed by measuring reflection spectrum $r_L(\omega\Gamma)$ of the lossy system for the left incidence. By tailoring losses Γ, both TEM and exceptional point (EP) of the scattering matrix [48] are first simultaneously observed, which builds a connection between topology and exceptional point (branch point associated with the coalescence of eigenvalues and the corresponding eigenvectors) in non-Hermitian system. Unidirectional reflectionless wave propagation ($r_L = 0$, $r_R \neq 0$) can be observed in Figs. 6(c)–6(f) when the critical condition $\Gamma = \Gamma_0$ is satisfied. Vortex-like pattern centered at zero reflection point in the reflection phase spectra is demonstrated in

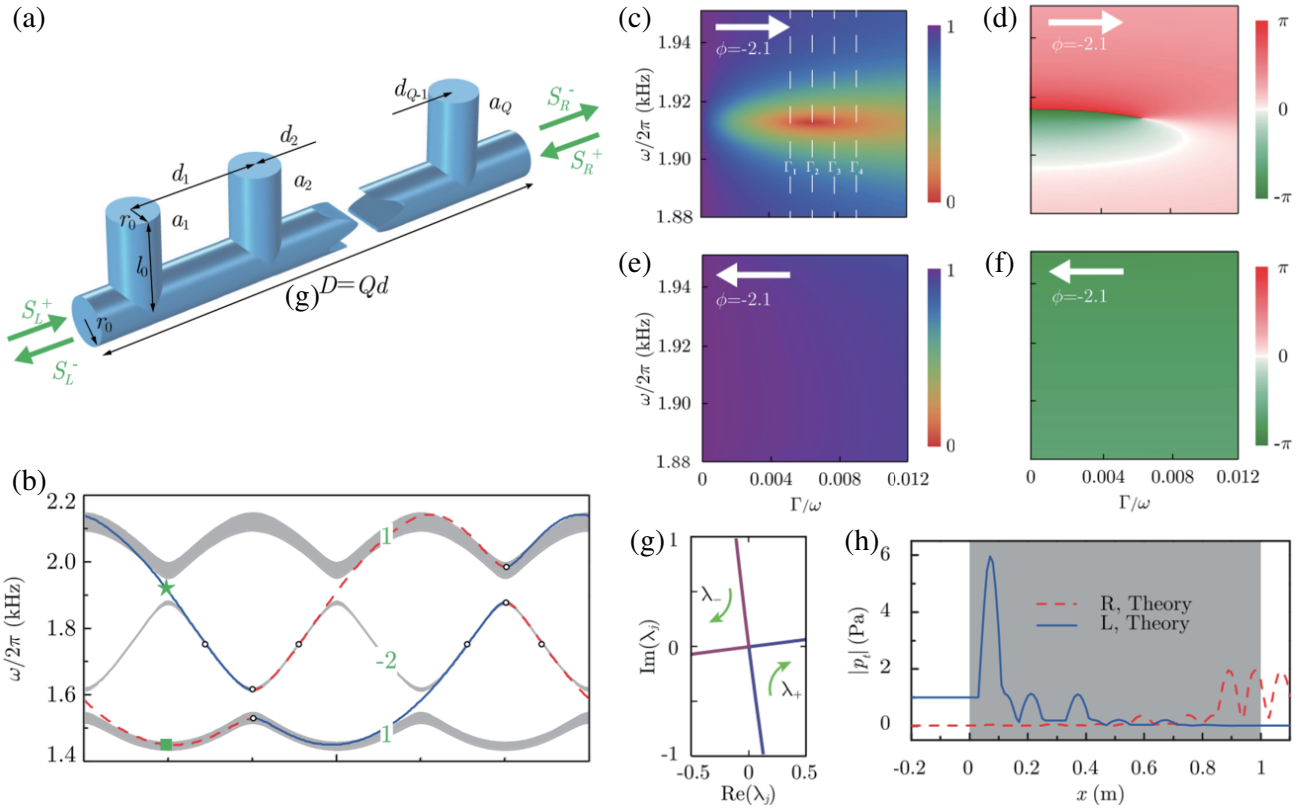

Figure 6. Simultaneous observation of a TEM and EP in 1D quasi-periodic system. (a) The schematic of the compound unit cell composed of a main tube with Q closed-end, side-branch tubes. (b) Projected band structure of the system without losses. The Chern number for each pass band is marked. The edge modes under left (right) incidence is illustrated with blue (red dashed) line. (c)–(h) The calculated reflectivity and reflection phase of the finite structure with $\phi = -2\pi/3$ (c), (d) for the left incidence and (e), (f) for the right incidence. (g) is the trajectories of eigenvalues λ in the complex plane with fixed frequency and varied losses Γ. (h) is the field distribution of system working at EP for left input and right input. Reproduced with permission from [16]. Copyright 2018 American Physical Society.

Fig. 6(d). According to the eigenvalue of the scattering matrix $\lambda = t \pm \sqrt{r_L r_R}$ shown in Fig. 6(g), it is obvious that here system is working at EP. The field distribution of system at EP is demonstrated in Fig. 6(h).

In this section, band topology and band inversion in various multi-scattering photonic systems have been reviewed from the perspective of effective electromagnetic parameters. Compared to the bulk-boundary correspondence theory in topology context, this idea gives a clear picture for the existence of TEMs satisfying impedance matching condition in 1D systems. It is later extended to 1D systems in hydrodynamics [49] and phononics [50]. Notably, these effective EM parameters of PCs are not real local ε and μ, as they only work well for wave propagation in that one dimension. In other words, this method remains to be improved when it comes to 2D problems such as incidence at different angles.

Both 1D and 2D photonic topological insulators (PTIs) are realized by lifting band degeneracy, and their band topologies are characterized by topological invariants such as Chern number or spin Chern number for 2D systems and Zak phase for 1D systems. For a composite structure consisting of two parts with distinct band topology, 1D or 2D topological edge modes which are robust to certain disorders and perturbations emerge at the interface between these two parts.

In general, 2D PTI can be achieved by breaking time reversal symmetry through applying magnetic field [5, 6, 11], or introducing pseudospin-orbit coupling [7, 8]. Take a specific case for example, pseudospin states can be introduced through polarizations (transverse magnetic and transverse electric

waves) [7]. Their linear combinations doubly degenerate under the condition $\hat{\varepsilon} = \hat{\mu}$ and can be taken as pseudospin states. Then a magneto-electric tensor χ acts on each state as a pseudospin-orbit coupling, and degeneracy is thus lifted. In contrast, neither magnetic field nor pseudospin-orbit coupling is essential for the aforementioned 1D PTI. Instead, we can build connections between effective mass m in 1D Dirac equation and effective ε, μ so that topological transition can be realized through sign change of m. The method is subsequently extended to photonic crystals and locally resonant metamaterials.

3. TOPOLOGICAL MODES IN DIMERIZED CHAIN BASED ON TIGHT BINDING MODEL

Topological photonics aims to develop robust optic modes which have been realized in array of near-field coupled resonators [34]. Such a structure is an analogue of SSH model in condensed matter physics.

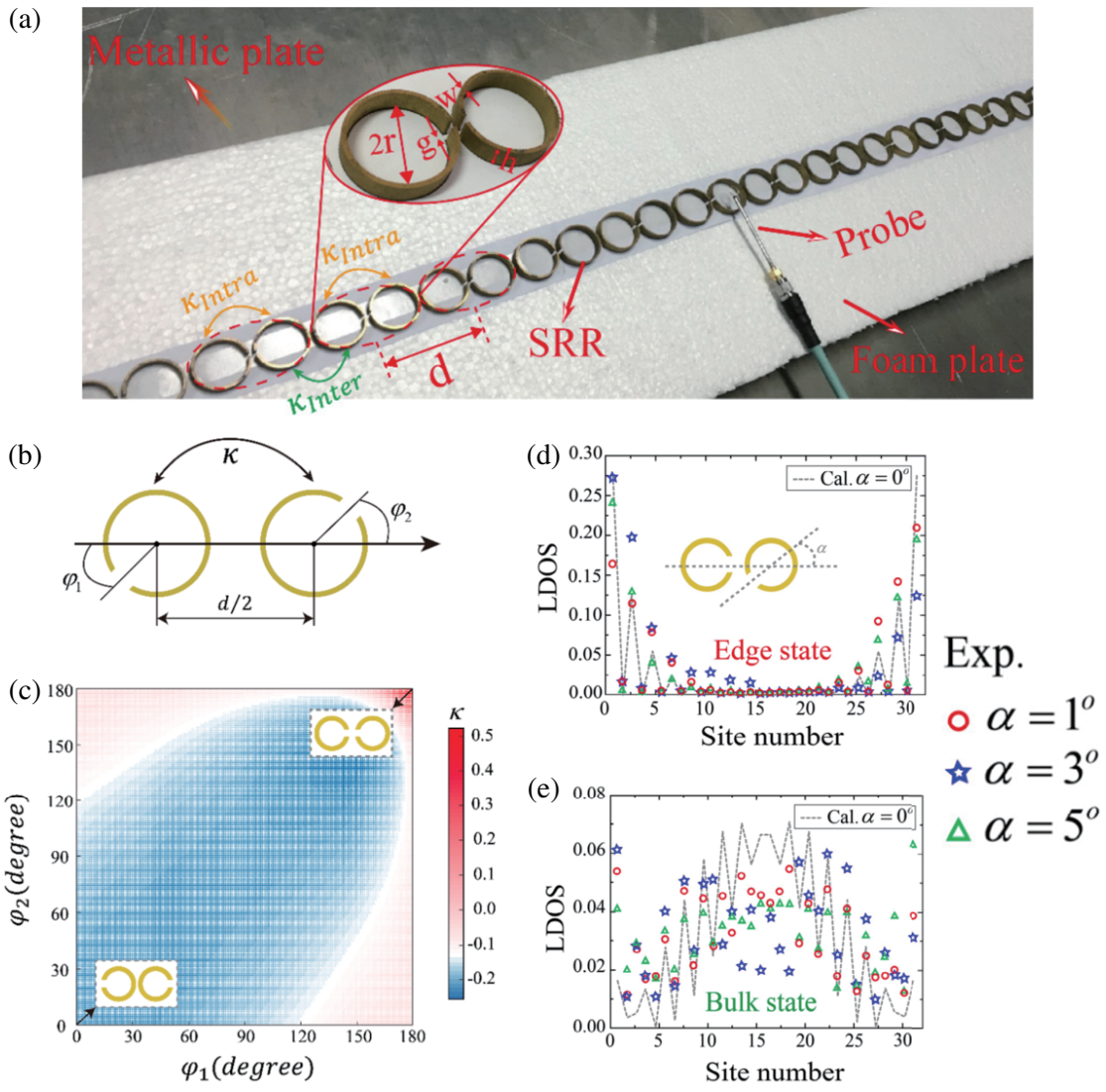

Figure 7. Experimental demonstration of the robust TEM in a dimerized SSR chain. (a) Experimental setup of the 1D dimer chain. (b) Sketch of a pair of arbitrarily rotated split rings. (c) Coupling strength versus the relevant angle between two rings. (d), (e) Measured and calculated LDOS distributions of the edge state (d) and the bulk state (e) at various disorder levels. Reproduced with permission from [51]. Copyright 2018 The Optical Society.

The SSH model describes electrons hopping on a chain. Consider a dimerized lattice with N unit cells, with each cell hosting two sites, A and B. Hopping amplitudes between adjacent sites are expressed as intracell and intercell coupling strength $\kappa_{intra} = u$ and $\kappa_{inter} = v$. The related Hamiltonian of the electron can be written as

$$H = u\sum_{n=1}^{N} a_n^{\dagger} b_n + v\sum_{n=1}^{N-1} b_n^{\dagger} a_{n+1}. \tag{4}$$

Here $a_n^{\dagger}(b_n^{\dagger})$ and $a_n(b_n)$ are the creation and annihilation operators of electron on sublattice site A (or B) in the n-th cell. State of the particle can be denoted as ψ_n.

For a finite chain, consider boundary condition (Born-Von Karman condition) $\psi_1 = \psi_{N+1}$ and perform the Fourier transformation, and the Hamiltonian can be rewritten as a 2×2 compact form

$$H(k) = \begin{pmatrix} 0 & d_x - id_y \\ d_x + id_y & 0 \end{pmatrix}, \tag{5}$$

which is also called bulk momentum-space Hamiltonian. Here $d_x = u + vcos(k)$, $d_y = vsin(k)$, $k \in [0, 2\pi]$. The eigenvalue equation of bulk Hamiltonian reads

$$H(k)\psi(k) = E(k)\psi(k), \tag{6}$$

where

$$\psi(k) = \begin{pmatrix} \alpha(k) \\ \beta(k) \end{pmatrix}. \tag{7}$$

The corresponding eigenvalues are $E(k) = \pm|dx + idy| = \pm d$. The phase angle of $d(k) = dx + idy$ is denoted as $\varphi(k)$. The dispersion relation of the bulk can thus be obtained from $E(k)$.

Generally speaking, the topology of SSH model can be determined from the existence of edge modes robust to disorders which is called TEMs. The topology of SSH model with $u < v$ differs from that of the system with $u > v$. Specifically, TEMs robust to disorders exist on both ends of the finite chain

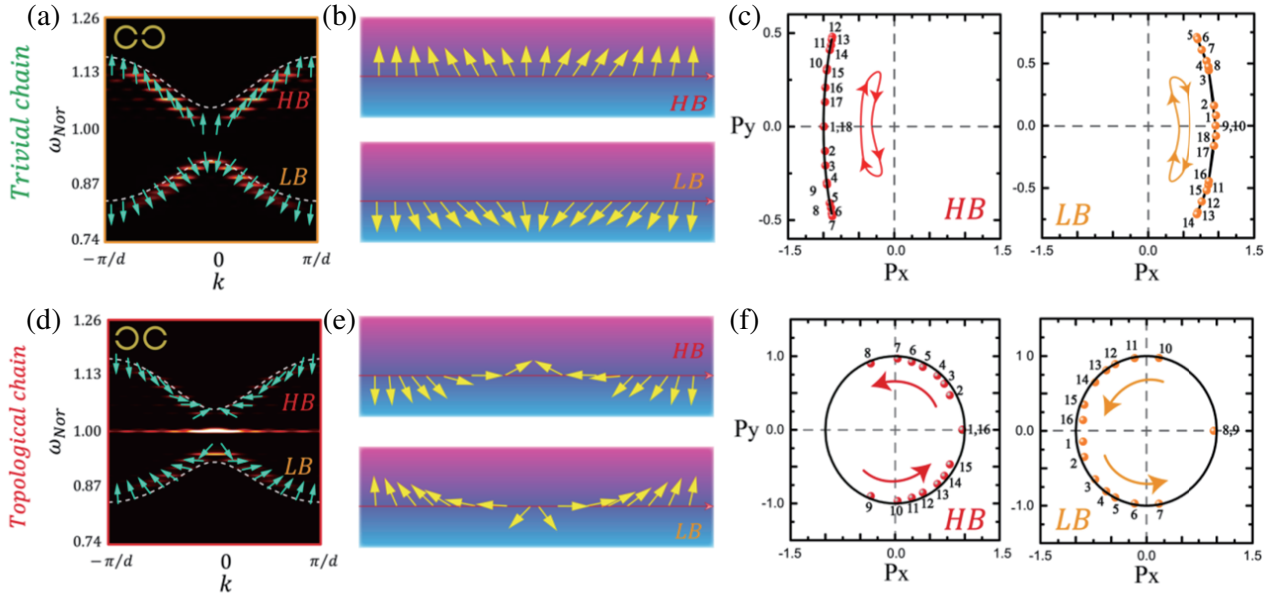

Figure 8. Seeing topological winding number and band inversion in dimerized chain of SRRs. (a) Calculated (dashed line) and measured dispersion relation of the trivial chain with pseudospin vectors. (b) Measured pseudospin vectors of bands in (a) are shown on the same horizontal line for better display. (c) Pseudospin vectors on the $PxOPy$ plane and the winding number that is indicated by the closed loops as the wave vector spans the 1st Brillouin zone. (d)–(f) similar to (a)–(c) but for the topological chain. Reproduced with permission from [55]. Copyright 2020 American Physical Society.

when $u < v$. From the perspective of band structure, SSH chain with $u > v(u < v)$ corresponds to trivial (topological) phase. Trivial (topological) phase is the state where system works before (after) closing of the band gap as u decreases from $u_{\max} = 2v$ to zero with v unchanged.

So, from the dispersion relation $E(k)$, it can be concluded that the topology is completely determined by relative magnitude of intracell coupling u and intercell coupling v. Topological properties of SSH model can be characterized by a topological invariant called Zak phase

$$\theta_{Zak} = \frac{1}{2}\int_{-\pi}^{\pi} d\varphi. \tag{8}$$

Compared with typical SSH model, disorders and perturbations can be accurately tuned in photonic artificial structures. In [34], the alternative coupling strength is controlled by the (straight) distance between resonators. Here we propose another method where coupling can be tuned with distance unchanged.

Jiang et al. observed TEM in SSH model experimentally in a dimer chain of SRRs, and the robustness of the TEM against disorder and losses is also verified [51]. The experimental setup of the dimer chain with identical SRRs is shown in Fig. 7(a). The coupling between SRRs can be manipulated

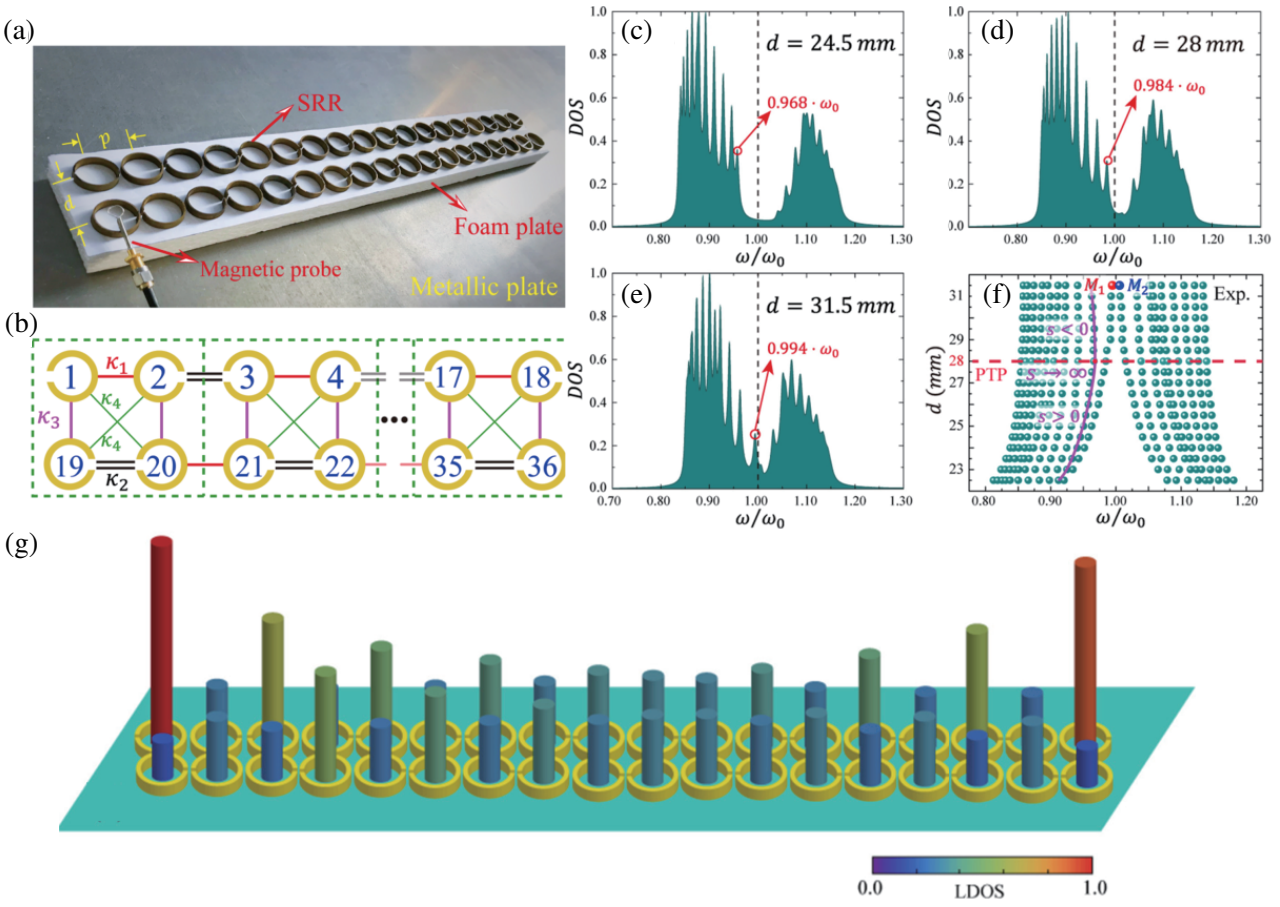

Figure 9. Observation of TEMs in an effective Kitaev chain composed of SRRs. (a) Photo of the Kitaev chain composed of two SRR chains. (b) Schematic model of the Kitaev chain. (c)–(e) Measured normalized DOS spectrum of the trivial (c)–(d) and topological (e) Kitaev chain. (f) Measured topological phase diagrams for the Kitaev chain. Dots are extracted from peaks in the different DOS spectrum. The lower band edge and the phase transition point (PTP) are marked by the solid line and dashed line, respectively. $s$represents the slope of the solid line. (g) The normalized LDOS distribution of the topological bound state [marked by $M1$ in (f)]. Reproduced with permission from [57]. Copyright 2021 American Physical Society.

through tuning the orientation angles of the slits of the SRRs instead of relative distance between them. Apparently, the coupling strength of the case whose gaps in neighboring SRRs are next to each other is stronger than the case whose gaps in neighboring SRRs are on opposite sides, as shown in Figs. 7(b) and 7(c). The density of states (DOSs) spectrum embodying band structure of the dimer chain is obtained by averaging the local density of states (LDOSs) spectrum over all sites, and the LDOS spectrum of each site is extracted from the reflection by a method of near-field detection [52]. As shown in Figs. 7(d) and 7(e), the edge mode is still maintained with different disorders realized by rotating SRRs, while the bulk state has been deteriorated seriously.

For 1D system, winding number is another topological invariant which can be directly obtained as $WN = \theta_{Zak}/\pi$ [35]. So far topological properties related to the winding number have been explored in lattices for ultra cold atoms [53] and acoustics [54], but direct measurement of winding numbers remains a challenge.

In 2020, a direct observation of winding number was first realized in such SRR chain system along with the measurement of dispersion relation, which reveals an important application of the SRR chain model [55]. The winding number of bands can be obtained by measuring the pseudospin vectors (P_x, P_y) in the chains, as shown in Fig. 8. Here, the sublattice pseudospin vector inversion observed at band edges indicates the band inversion in topological chain and the associated topological transition. On the other hand, the dynamic structure factor [56] embodying dispersion relation can be determined from the surface current distribution that can be obtained by the aforementioned method of near-field detection. The normalized current distributions of band-edge modes for the trivial and topological dimer chains are also investigated in order to verify the connection between switched symmetry of band-edge states and band inversion.

With the introduction of the concept of synthetic dimension, a Kitaev model is realized in a double SSH chain structure illustrated in Figs. 9(a), 9(b), and TEMs in non-trivial Kitaev chain are depicted in Fig. 9(g) [57]. The topological transition is achieved by tuning the distance d between two chains, which is shown in Figs. 9(c), 9(f). Furthermore, by inserting a trivial chain into a topological chain, the coupling of two TEMs is realized through tuning the length of the inserted chain, which has a potential application in non-Hermitian systems.

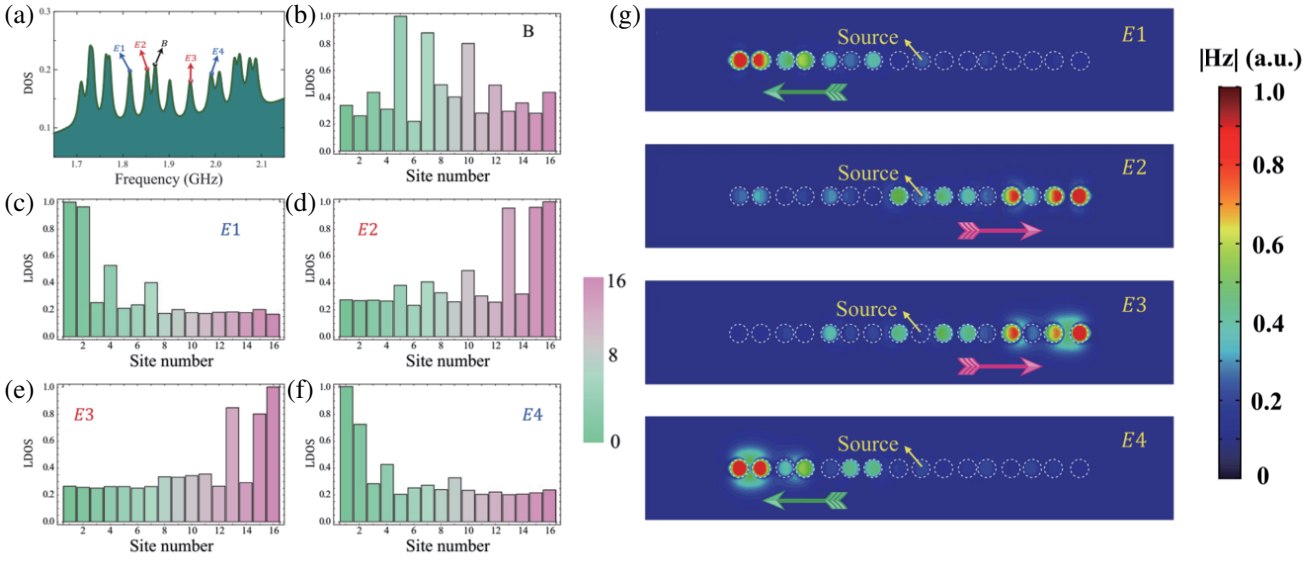

Figure 10. symmetric TEMs in a Harper chain composed of SRRs. (a) Measured DOS spectrum of the topological Harper chain. Four edge states exsiting in two gaps separately (E1–E4) and one bulk state are marked by the arrows. (b)–(f) Measured LDOS distribution of the bulk state (b) and four edge states (c)–(f). (g) Selective unidirectional power transfer based on the topological Harper chain. Adapted with permission from [58]. Copyright 2018 The Optical Society.

This photonic SSH model with accurately tunable coupling can also be applied to investigate topological properties of quasi-periodic tight binding systems. In 2018, such a design was extended to a Harper model (also known as the AAH model). It is demonstrated in Figs. 10(a)–10(f) that two topological modes with different energies can be found in one band gap of a Harper chain, and interestingly, these two modes distribute on either end of the chain [58]. When the length of the chain is changed with the left end fixed, the mode on the left end is preserved. This phenomenon is experimentally investigated with the SRR chain, which is illustrated in Fig. 10(g). Asymmetric transmission may be realized on account of such a feature.

4. NOVEL APPLICATION OF TOPOLOGICAL EDGE MODES

The research on TEMs in 2D systems has sparked the development of novel topological photonic devices including topological insulator laser and robust optical delay lines [9, 10, 59]. When it comes to 1D topological system, an innovative technology called topological wireless power transfer (TWPT) has attracted great interest in the last two years. This latest application of dimer chain model stems from an amazing combination of TEMs in dimer chain and Parity-Time (PT) symmetric wireless power transfer (WPT) system based on resonant coils [60, 61].

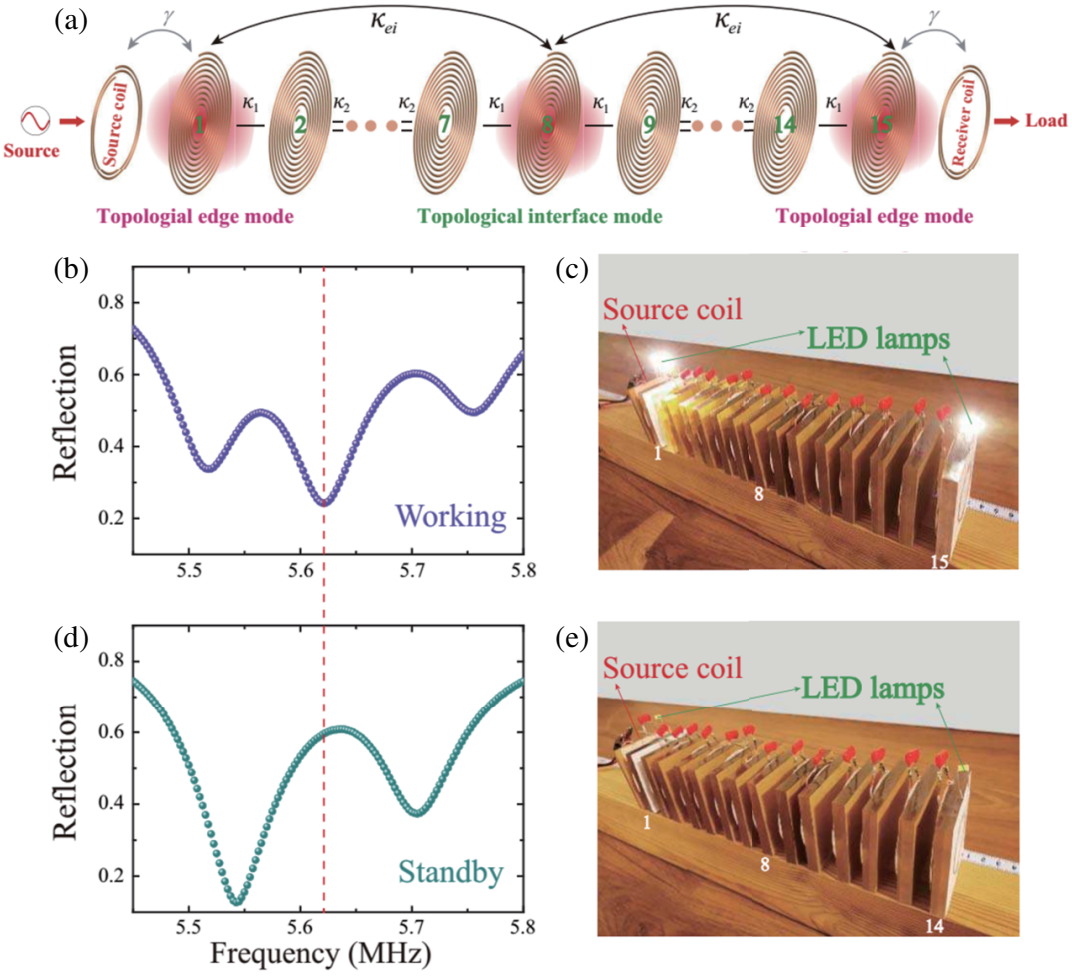

Figure 11. Topological WPT. (a) Scheme of a TWPT system based on the effective third-order PT symmetry. (b)–(c) Measured reflection spectrum (b) and experimental demonstration (c) of TWPT. (d)–(e) Similar to (b), (c), but for the standby state. Reproduced with permission from [60]. Copyright 2021 American Physical Society.

Song et al. [60] experimentally verify that the TEMs in the effective two-state PT system based on a dimer chain composed of ultrasubwavelength resonators are immune to the inner disorder perturbation and can be used to realize the long-range TWPT with high transmission efficiency. The schematic of the system is illustrated in Fig. 11(a). Here, two coupled TEMs with source and load at the end of the chain can be regarded as two identical resonators in a two-state PT system. Source acts as an effective gain [62]. Furthermore, in order to solve the tricky technical problems of standby power loss and frequency tracking in effective two-state PT system, a WPT system with effective triple-state PT symmetry is constructed by taking one topological interface mode and two TEMs as triple resonators. The reflection spectrum and experimental demonstration of TWPT are shown in Figs. 11(b)–11(e).

Directional WPT based on actively controlled TEMs in quasiperiodic Harper chain is demonstrated in Fig. 12 [63]. By adding active elements (variable capacitance diodes with applied voltage U) into the topological quasiperiodic chain, the resonant frequency of the resonators can be flexibly controlled, which makes the original edge mode on the right end become edge mode on the left end. The change of transmission direction is observed clearly, which implies the directional WPT. In addition, it is verified

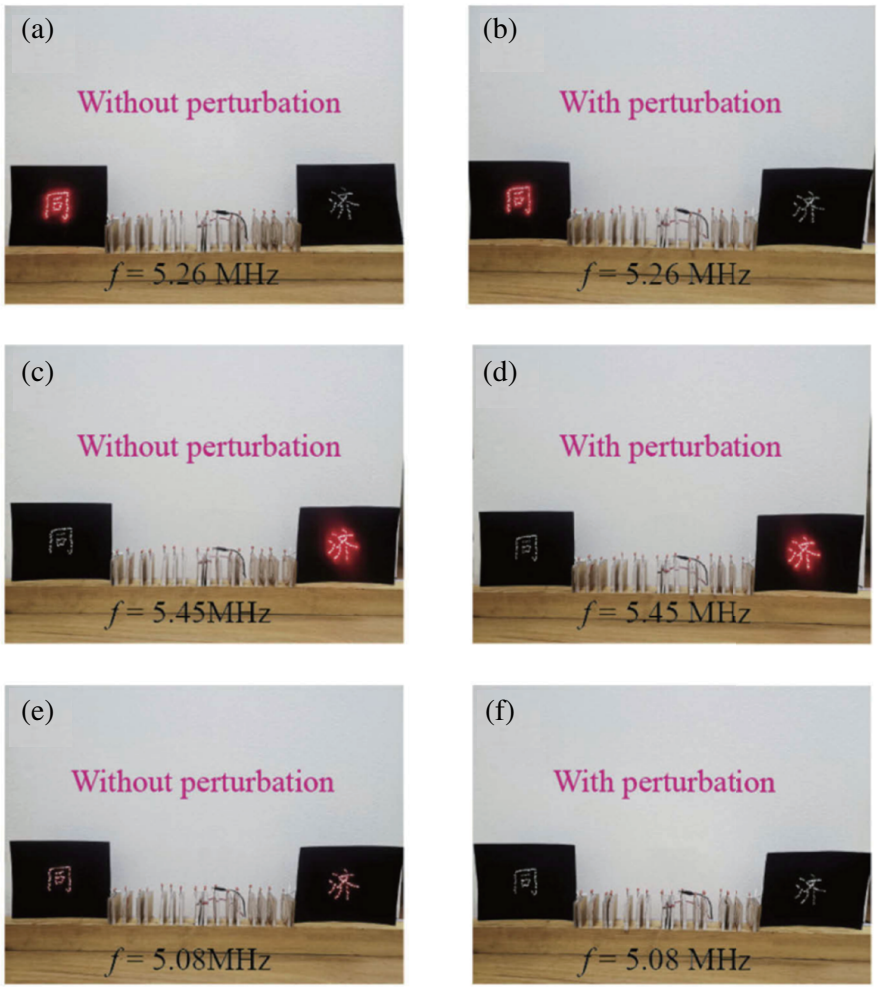

Figure 12. Experimental demonstration of the directional WPT for lighting two Chinese characters 'tong' and 'ji' with LED lamps. The non-resonant source coil is placed at the center of the chain. (a), (c), (e) WPT system working at the left TEM (a), the right TEM (c) and bulk state (e). (b), (d), (f) Similar to (a), (c), (e), but for the topological Harper chain with perturbation. Reproduced with permission from [63]. Copyright 2021 The Optical Society.

that the WPT system based on TEMs in Harper chain is robust against certain disorders in coupling, which can be very useful in real-life scenarios such as the robots whose structure will often deform.

The potential application of SSH chain in EP-enhanced sensing is also discussed recently. Compared to traditional sensor based on diabolic point in Hermitian system where eigenfrequency splitting $\delta\omega$ has a linear relationship with the perturbation ε, $\delta\omega$ is proportional to square root of ε when the sensor operates at EP in a non-Hermitian system. Therefore, for sufficiently small ε, $\delta\omega$ is greatly enhanced for sensors operating at EP [62, 64–66]. In a recent work, effective two-state PT system (Fig. 13(a)) is constructed by adding physical gain and loss to both ends of a finite dimer chain where the coupling of two TEMs is involved [67]. As shown in Fig. 13(b), two TEMs coalesce at EP by tuning the loss of the resonator on the right end. It is demonstrated in Fig. 13(c) that $\delta\omega$ is proportional to square root of small perturbation in the lossy resonator if and only if the system is working at EP. More importantly, it is shown in Fig. 13(d) that the system is robust to disorders in site-to-site couplings, which is a novel design compared to common EP-enhanced sensor sensitive to fabrication error.

Apart from these applications, the utilizations of topological modes in optics have also been investigated. For instance, a TEM with a high reflectance in photonic heterostructure composed of

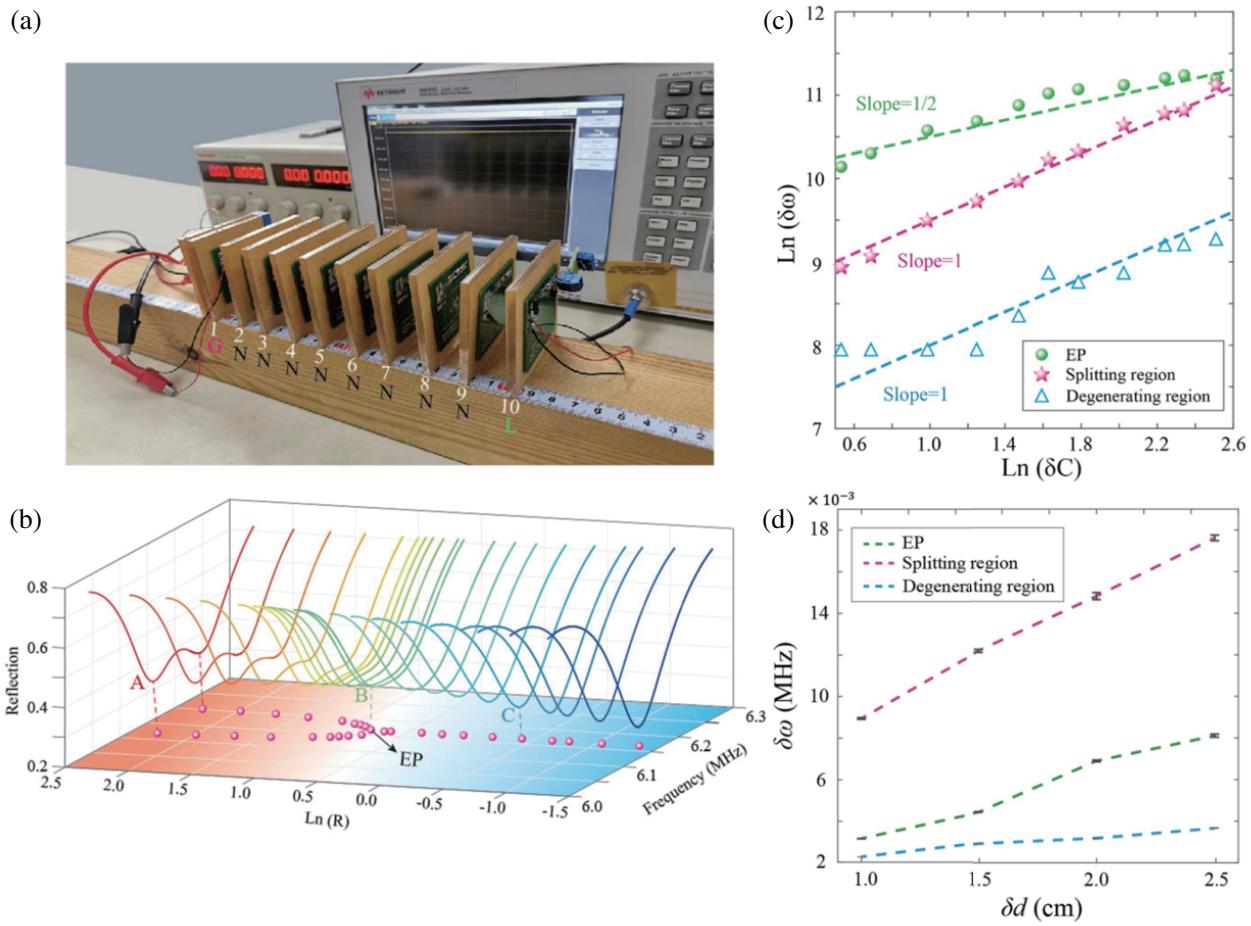

Figure 13. Topological sensor based on 1D non-Hermitian dimer chain. (a) Photo of the setup. (b) Measured reflection spectrum with varied resistance R. Dots denote the frequencies of the edge states. Resistance is given on a logarithmic scale. (c) Measured frequency splitting of edge states versus frequency detuning of the right resonator controlled by the loaded capacitors. (d) Frequency splitting as a function of disorder strength in the dimer chain. The disorder is introduced by randomly moving four coil resonators at different distance δd in the center of the chain. Reproduced with permission from [67]. Copyright 2021 Chinese Laser Press.

two different all-dielectric PCs with symmetric unit cells is proposed, and Giant Goos-Hanchen shift enhancement is achieved [68]. Such an effect can be utilized to design ultrasensitive sensors.

Another kind of topological mode, called topological Tamm mode, has also been exploited in the past few years. A topological Tamm mode exists at the interface between metal with negative reflection phase and a PC with positive reflection phase [69]. The enhancement of Faraday rotation effect [70] and optical nonlinearity [71] are realized based on such topological mode.

5. CONCLUSION AND OUTLOOK

We have reviewed the recent advance in TEMs in electromagnetic systems. It has been proposed that Maxwell's equations can be explicitly mapped to the Dirac equation in one dimension, which leads to the establishment of the connection between effective electromagnetic parameters and topological orders. Such a connection together with TEMs is verified in various photonic artificial structures including PCs, TL metamaterials, and locally resonant metamaterials. We have also discussed TEMs and investigated their applications in energy transfer, sensing, and field of optics.

These results may be extended to other platforms such as acoustics and circuits. It is notable that novel topological phenomena in more sophisticated systems constructed by introducing non-Hermiticity and disorder into plain SSH model have gained great attention in recent years.

5.1. Skin Effect

The introduction of non-Hermiticity into topological system leads to a breakdown of common bulk-edge correspondence. TEMs can be found at the boundary of a Hermitian open chain, while all the bulk states are found to be localized near boundary of the chain in the non-Hermitian case [72]. Such a phenomenon is called the non-Hermitian skin effect. The non-Hermitian skin effect has recently been theoretically discussed in 1D tight-binding model [73–75] and experimentally observed in circuits [76]. The relationship between TEM and skin effects has also been explored [77]. Subsequently, a topological sensor immune to local perturbations based on skin effect and TEMs [78] is proposed as an application, with more applications remaining to be discovered.

5.2. Edge Mode in Topological Anderson Insulator

Common topological insulators usually become trivial insulators for sufficiently strong disorders. In contrast, disorders can induce the nontrivial phase from the trivial phase, and the disorder-induced nontrivial phase is known as topological Anderson insulator (TAI) [79]. TAIs have been theoretically investigated in systems including HgTe/CdTe quantum wells [79], Haldane model in circuits [80], photonic lattice [81], photonic crystal [82], and SSH chain based on ultracold atoms [83]. The integration of TAIs and non-Hermiticity has also been exploited in the past few years [84].

ACKNOWLEDGMENT

We acknowledge the support from the National Key Research Program of China (Grant No. 2021YFA1400602), the National Natural Science Foundation of China (Grants No. 91850206, 11974261), and the Fundamental Research Funds for the Central Universities (Grant No. 22120210579).

REFERENCES

1. Hasan, M. Z. and C. L. Kane, "Colloquium: Topological insulators," *Reviews of Modern Physics*, Vol. 82, No. 4, 3045–3067, 2010.
2. Qi, X.-L. and S.-C. Zhang, "Topological insulators and superconductors," *Reviews of Modern Physics*, Vol. 83, No. 4, 1057–1110, 2011.
3. Lu, L., J. D. Joannopoulos, and M. Soljačić, "Topological photonics," *Nature Photonics*, Vol. 8, No. 11, 821–829, 2014.

4. Haldane, F. D. M. and S. Raghu, "Possible realization of directional optical waveguides in photonic crystals with broken time-reversal symmetry," *Physical Review Letters*, Vol. 100, No. 1, 013904, 2008.
5. Wang, Z., Y. D. Chong, J. D. Joannopoulos, and M. Soljačić., "Observation of unidirectional backscattering-immune topological electromagnetic states," *Nature*, Vol. 461, No. 7265, 772–775, 2009.
6. Hafezi, M., S. Mittal, J. Fan, A. Migdall, and J. M. Taylor, "Imaging topological edge states in silicon photonics," *Nature Photonics*, Vol. 7, No. 12, 1001–1005, 2013.
7. Khanikaev, A. B., et al., "Photonic topological insulators," *Nature Materials*, Vol. 12, No. 3, 233–239, 2013.
8. Wu, L. H. and X. Hu, "Scheme for achieving a topological photonic crystal by using dielectric material," *Physical Review Letters*, Vol. 114, No. 22, 223901, 2015.
9. Harari, G., M. A. Bandres, Y. Lumer, M. C. Rechtsman, Y. D. Chong, M. Khajavikhan, D. N. Christodoulides, and M. Segev, "Topological insulator laser: Theory," *Science*, Vol. 359, No. 6381, eaar4003, 2018.
10. Bandres, M. A., S. Wittek, G. Harari, M. Parto, J. Ren, M. Segev, D. N. Christodoulides, and M. Khajavikhan, "Topological insulator laser: Experiments," *Science*, Vol. 359, No. 5381, eaar4005, 2018.
11. Rechtsman, M. C., et al., "Photonic Floquet topological insulators," *Nature*, Vol. 496, No. 7444, 196–200, 2013.
12. Lin, H. and L. Lu, "Dirac-vortex topological photonic crystal fibre," *Light: Science & Applications*, Vol. 9, No. 1, 202, 2020.
13. Joannopoulos, J. D., S. G. Johnson, J. N. Winn, and R. D. Meade, *Photonic Crystals: Molding the Flow of Light*, Princeton University Press, 2nd Edition, 2008.
14. Yablonovitch, E., "Inhibited spontaneous emission in solid-state physics and electronics," *Physical Review Letters*, Vol. 58, No. 20, 2059–2062, 1987.
15. John, S., "Strong localization of photons in certain disordered dielectric superlattices," *Physical Review Letters*, Vol. 58, No. 23, 2486–2489, 1987.
16. Zhu, W., X. Fang, D. Li, Y. Sun, Y. Li, Y. Jing, and H. Chen, "Simultaneous observation of a topological edge state and exceptional point in an open and non-Hermitian acoustic system," *Physical Review Letters*, Vol. 121, No. 12, 124501, 2018.
17. Zhu, S. and X. Zhang, "Metamaterials: artificial materials beyond nature," *National Science Review*, Vol. 5, No. 2, 131–131, 2018.
18. Pendry, J. B., "Negative refraction makes a perfect lens," *Physical Review Letters*, Vol. 85, No. 18, 3966–3969, 2000.
19. Ahn, D., J. Park, C. Kim, J. Kim, Y. Qian, and T. Itoh, "A design of the low-pass filter using the novel microstrip defected ground structure," *IEEE Transactions on Microwave Theory and Techniques*, Vol. 49, No. 1, 86–93, 2001.
20. Pendry, J. B., D. Schurig, and D. R. Smith, "Controlling electromagnetic fields," *Science*, Vol. 312, No. 5781, 1780–1782, 2006.
21. Schurig, D., J. J. Mock, B. J. Justice, S. A. Cummer, J. B. Pendry, A. F. Starr, and D. R. Smith, "Metamaterial electromagnetic cloak at microwave frequencies," *Science*, Vol. 314, No. 5801, 977–980, 2006.
22. Fang, N., H. Lee, C. Sun, and X. Zhang, "Sub-diffraction-limited optical imaging with a silver superlens," *Science*, Vol. 308, No. 5721, 534–537, 2005.
23. Cui, T. J., M. Q. Qi, X. Wan, J. Zhao, and Q. Cheng, "Coding metamaterials, digital metamaterials and programmable metamaterials," *Light: Science & Applications*, Vol. 3, e218, 2014.
24. Liu, W., Z. N. Chen, and X. Qing, "Metamaterial-based low-profile broadband mushroom antenna," *IEEE Transactions on Antennas and Propagation*, Vol. 62, No. 3, 1165-1172, 2014.

25. Hao, J., Y. Yuan, L. Ran, T. Jiang, J. A. Kong, C. T. Chan, and L. Zhou, "Manipulating electromagnetic wave polarizations by anisotropic metamaterials," *Physical Review Letters*, Vol. 99, No. 6, 063908, 2007.
26. Cai, T., et al., "High-efficiency and full-space manipulation of electromagnetic wave fronts with metasurfaces," *Physical Review Applied*, Vol. 8, No. 3, 034033, 2017.
27. Su, W. P., J. R. Schrieffer, and A. J. Heeger, "Solitons in polyacetylene," *Physical Review Letters*, Vol. 42, No. 25, 1698–1701, 1979.
28. Malkova, N., I. Hromada, X. Wang, G. Bryant, and Z. Chen, "Observation of optical Shockley-like surface states in photonic superlattices," *Optics Letters*, Vol. 34, No. 11, 1633–1635, 2009.
29. Tan, W., Y. Sun, H. Chen, and S.-Q. Shen, "Photonic simulation of topological excitations in metamaterials," *Scientific Reports*, Vol. 4, 3842, 2014.
30. Poshakinskiy, A. V., A. N. Poddubny, L. Pilozzi, and E. L. Ivchenko, "Radiative topological states in resonant photonic crystals," *Physical Review Letters*, Vol. 112, No. 10, 107403, 2014.
31. Xiao, M., Z. Q. Zhang, and C. T. Chan, "Surface impedance and bulk band geometric phases in one-dimensional systems," *Physical Review X*, Vol. 4, No. 2, 021017, 2014.
32. Poddubny, A., A. Miroshnichenko, A. Slobozhanyuk, and Y. Kivshar, "Topological Majorana states in zigzag chains of plasmonic nanoparticles," *ACS Photonics*, Vol. 1, No. 2, 101–105, 2014.
33. Ling, C. W., M. Xiao, S. F. Yu, and K. H. Fung, "Topological edge plasmon modes between diatomic chains of nanoparticles," *Optics Express*, Vol. 23, No. 3, 2021–2031, 2015.
34. Poli, C., M. Bellec, U. Kuhl, F. Mortessagne, and H. Schomerus, "Selective enhancement of topologically induced interface states," *Nature Communications*, Vol. 6, 6710, 2015.
35. Shen, S. Q., *Topological Insulators: Dirac Equation in Condensed Matter*, 2nd Edition, Springer, 2017.
36. Guan, G., H. Jiang, H. Li, Y. Zhang, H. Chen, and S. Y. Zhu, "Tunneling modes of photonic heterostructures consisting of single-negative materials," *Applied Physics Letters*, Vol. 88, No. 21, 211112, 2006.
37. Guo, J., H. Chen, H. Li, and Y. Zhang, "Effective permittivity and permeability of one dimensional dielectric photonic crystal within a band gap," *Chinese Physics B*, Vol. 17, No. 7, 2544–2552, 2008.
38. Shi, X., C. Xue, H. Jiang, and H. Chen, "Topological description for gaps of one-dimensional symmetric all-dielectric photonic crystals," *Optics Express*, Vol. 24, No. 16, 18580–18581, 2016.
39. Huang, Q., Z. Guo, J. Feng, C. Yu, H. Jiang, Z. Zhang, Z. Wang, and H. Chen, "Observation of a topological edge state in the X-ray band," *Laser & Photonics Reviews*, Vol. 13, No. 6, 1800339, 2019.
40. Wang, Q., M. Xiao, H. Liu, S. N. Zhu, and C. T. Chan, "Measurement of the Zak phase of photonic bands through the interface states of a metasurface/photonic crystal," *Physical Review B*, Vol. 93, No. 4, 041415, 2016.
41. Lemoult, F., N. Kaina, M. Fink, and G. Lerosey, "Wave propagation control at the deep subwavelength scale in metamaterials," *Nature Physics*, Vol. 9, No. 1, 55–60, 2013.
42. Fan, L., W. W. Yu, S. Y. Zhang, H. Zhang, and J. Ding, "Zak phases and band properties in acoustic metamaterials with negative modulus or negative density," *Physical Review B*, Vol. 94, No. 17, 174307, 2016.
43. Zhu, W., Y.-Q. Ding, J. Ren, Y. Sun, Y. Li, H. Jiang, and H. Chen, "Zak phase and band inversion in dimerized one-dimensional locally resonant metamaterials," *Physical Review B*, Vol. 97, No. 19, 195307, 2018.
44. Fan, C., X. Shi, F. Wu, Y. Li, H. Jiang, Y. Sun, and H. Chen, "Photonic topological transition in dimerized chains with the joint modulation of near-field and far-field couplings," *Photonics Research*, Vol. 10, No. 1, 41–49, 2022.
45. Verbin, M., O. Zilberberg, Y. E. Kraus, Y. Lahini, and Y. Silberberg, "Observation of topological phase transitions in photonic quasicrystals," *Physical Review Letters*, Vol. 110, No. 7, 076403, 2013.
46. Lang, L., X. Cai, and S. Chen, "Edge states and topological phases in one-dimensional optical superlattices," *Physical Review Letters*, Vol. 108, No. 21, 220401, 2012.

47. Kraus, Y. E., Y. Lahini, Z. Ringel, M. Verbin, and O. Zilberberg, "Topological states and adiabatic pumping in quasicrystals," *Physical Review Letters*, Vol. 109, No. 10, 106402, 2012.
48. Feng, L., Y.-L. Xu, W. S. Fegadolli, M.-H. Lu, J. E. B. Oliveira, V. R. Almeida, Y.-F. Chen, and A. Scherer, "Experimental demonstration of a unidirectional reflectionless parity-time metamaterial at optical frequencies," *Nature Materials*, Vol. 12, No. 2, 108–113, 2013.
49. Shi, X., Y. Sun, C. Xue, and X. Hu, "Prediction of interface states in liquid surface waves with one-dimensional modulation," *Physics Letters A*, Vol. 383, No. 17, 2106–2109, 2019.
50. Zhang, D., J. Ren, T. Zhou, and B. Li, "Dark state, zero-index and topology in phononic metamaterials with negative mass and negative coupling," *New Journal of Physics*, Vol. 21, 093033, 2019.
51. Jiang, J., Z. W. Guo, Y. Q. Ding, Y. Sun, Y. H. Li, H. T. Jiang, and H. Chen, "Experimental demonstration of the robust edge states in a split-ring-resonator chain," *Optics E xpress*, Vol. 26, No. 10, 12891–12902, 2018.
52. Bellec, M., U. Kuhl, G. Montambaux, and F. Mortessagne, "Tight-binding couplings in microwave artificial graphene," *Physical Review B*, Vol. 88, No. 11, 115437, 2013.
53. Atala, M., M. Aidelsburger, J. T. Barreiro, D. Abanin, T. Kitagawa, E. Demler, and I. Bloch, "Direct measurement of the Zak phase in topological Bloch bands," *Nature Physics*, Vol. 9, No. 12, 795–800, 2013.
54. Xiao, M., G. Ma, Z. Yang, P. Sheng, Z. Q. Zhang, and C. T. Chan, "Geometric phase and band inversion in periodic acoustic systems," *Nature Physics*, Vol. 11, No. 3, 240–244, 2015.
55. Jiang, J., J. Ren, Z. W. Guo, W. W. Zhu, Y. Long, H. T. Jiang, and H. Chen, "Seeing topological winding number and band inversion in photonic dimer chain of split-ring resonators," *Physical Review B*, Vol. 101, No. 16, 165427, 2020.
56. Ashcroft, N. W. and N. D. Mermin, "Solid state physics," *Saunders College Publishing*, 1976.
57. Guo, Z. W., J. Jiang, H. T. Jiang, J. Ren, and H. Chen, "Observation of topological bound states in a double Su-Schrieffer-Heeger chain composed of split ring resonators," *Physical Review Research*, Vol. 3, No. 1, 013122, 2021.
58. Guo, Z. W., H. T. Jiang, Y. Sun, Y. H. Li, and H. Chen, "Asymmetric topological edge states in a quasiperiodic Harper chain composed of split-ring resonators," *Optics Letters*, Vol. 43, No. 20, 5142–5145, 2018.
59. Hafezi, M., E. A. Delmer, M. D. Lukin, and J. M. Taylor, "Robust optical delay lines with topological protection," *Nature Physics*, Vol. 7, No. 11, 907–912, 2011.
60. Song, J., F. Yang, Z. Guo, X. Wu, K. Zhu, J. Jiang, Y. Sun, Y. Li, H. Jiang, and H. Chen, "Wireless power transfer via topological modes in dimer chains," *Physical Review Applied*, Vol. 15, No. 1, 014009, 2021.
61. Zhang, L. et al., "Demonstration of topological wireless power transfer," *Science Bulletin*, Vol. 66, No. 10, 974–980, 2021.
62. Zeng, C., Y. Sun, G. Li, Y. Li, H. Jiang, Y. Yang, and H. Chen, "Enhanced sensitivity at high-order exceptional points in a passive wireless sensing system," *Optics Express*, Vol. 27, No. 20, 27562–27572, 2019.
63. Yang, F., et al., "Actively controlled asymmetric edge states for directional wireless power transfer," *Optics Express*, Vol. 29, No. 5, 7844–7857, 2021.
64. Hodaei, H., A. U. Hassan, S. Wittek, H. Garcia-Gracia, R. El-Ganainy, D. N. Christodoulides, and M. Khajavikhan, "Enhanced sensitivity at higher-order exceptional points," *Nature*, Vol. 548, No. 7666, 187–191, 2017.
65. Chen, W. J., S. K. Ozdemir, G. M. Zhao, J. Wiersig, and L. Yang, "Exceptional points enhance sensing in an optical microcavity," *Nature*, Vol. 548, No. 7666, 192–196, 2017.
66. Chen, P. Y. and R. El-Ganainy, "Exceptional points enhance wireless readout," *Nature Electronics*, Vol. 2, 323–324, 2019.
67. Guo, Z. W., T. Zhang, J. Song, H. Jiang, and H. Chen, "Sensitivity of topological edge states in a non-Hermitian dimer chain," *Photonics Research*, Vol. 9, No. 4, 574–582, 2021.

68. Wu, J., F. Wu, K. Lv, Z. Guo, H. Jiang, Y. Sun, Y. Li, and H. Chen, "Giant Goos-Hanchen shift with a high reflectance assisted by interface states in photonic heterostructures," *Physical Review A*, Vol. 101, No. 5, 053838, 2020.
69. Wang, Q., M. Xiao, H. Liu, S. Zhu, and C. T. Chan, "Optical interface states protected by synthetic weyl points," *Physical Review X*, Vol. 7, No. 3, 031032, 2017.
70. Dong, L., H. Jiang, H. Chen, and Y. Shi, "Enhancement of Faraday rotation effect in heterostructures with magneto-optical metals," *Journal of Applied Physics*, Vol. 107, No. 9, 093101, 2010.
71. Du, G., H. Jiang, Z. Wang, and H. Chen, "Optical nonlinearity enhancement in heterostructures with thick metallic film and truncated photonic crystals," *Optics Letters*, Vol. 34, No. 5, 578–580, 2009.
72. Bergholtz, E. J., J. C. Budich, and F. K. Kunst, "Exceptional topology of non-Hermitian systems," *Review of Modern Physics*, Vol. 93, No. 1, 015005, 2021.
73. Yao, S. Y. and Z. Wang, "Edge states and topological invariants of non-Hermitian systems," *Physical Review Letters*, Vol. 121, No. 8, 086803, 2018.
74. Lee, T. E., "Anomalous edge state in a non-Hermitian lattice," *Physical Review Letters*, Vol. 116, No. 13, 133903, 2016.
75. Xiong, Y., "Why does bulk boundary correspondence fail in some non-Hermitian topological models" *Journal of Physics Communications*, Vol. 2, No. 3, 035043, 2018.
76. Helbig, T., et al., "Generalized bulk-boundary correspondence in non-Hermitian topolectrical circuits," *Nature Physics*, Vol. 16, No. 7, 747, 2020.
77. Okuma, N. and M. Sato, "Hermitian zero modes protected by nonnormality: application of pseudospectra," *Physical Review B*, Vol. 102, No. 1, 014203, 2020.
78. Budich, J. C. and E. J. Bergholtz, "Non-Hermitian topological sensors," *Physical Review Letters*, Vol. 125, No. 18, 180403, 2020.
79. Li, J., R. Chu, J. Jain, and S.-Q. Shen, "Topological anderson insulator," *Physical Review Letters*, Vol. 102, No. 13, 136806, 2009.
80. Zhang, Z., B. Wu, J. Song, and H. Jiang, "Topological anderson insulator in electric circuits," *Physical Review B*, Vol. 100, No. 18, 184202, 2019.
81. Stutzer, S., et al., "Photonic topological Anderson insulators," *Nature*, Vol. 560, 461-465, 2018.
82. Liu, G., e al., "Topological Anderson insulator in disordered photonic crystals," *Physical Review Letters*, Vol. 125, No. 13, 133603, 2020.
83. Meier, E. J., F. A. An, A. Dauphin, M. Maffei, P. Massignan, T. L. Hughes, and B. Gadway, "Observation of the topological Anderson insulator in disordered atomic wires," *Science*, Vol. 362, 929, 2018.
84. Lin, Q., T. Lin, L. Xiao, K. Wang, W. Yi, and P. Xue, "Observation of non-Hermitian topological Anderson insulator in quantum dynamics," *Nature Communications*, Vol. 13, 3229, 2022.